

Possible electromagnetic signatures of coalescing neutron – black hole binaries

K.A. Postnov^{1,2,3}, A.G. Kuranov^{1,4}, I.V. Simkin⁵

¹ Sternberg Astronomical Institute, Universitetskij pr. 13, 119234 Moscow, Russia

² Institute of Experimental and Theoretical Physics, B. Cheremushkinskaya 25, 117218 Moscow, Russia

³ Faculty of Physics, Novosibirsk University, Pirogova 2, 630090 Novosibirsk, Russia

⁴ Foreign Trade Academy, Pudovkina 4a, 119285 Moscow, Russia

⁵ Baumann Moscow Technical University, 2d Baumanskaya 5, 105005 Moscow, Russia

Abstract

Possible models for the generation of electromagnetic (EM) radiation during the coalescence of neutron starblack hole binaries are considered. The mass of the remnant disk around the black hole during the coalescence of neutron stars and black holes is calculated by taking into account the equation of state for neutron stars and the rotation of the binary components before the coalescence. The parameters of binary systems before the coalescence (the mass ratio, the component rotation, the neutron star magnetic field) are calculated by the population synthesis method. The derived mass of the remnant disk around the black hole after the coalescence is used to estimate the kinetic energy of the relativistic jet launched by the BlandfordZnajek mechanism. A disk mass of more than $\sim 0.05M_{\odot}$ required for the formation of short gamma-ray bursts is shown to be obtained in no more than 1-10% of the coalescences (depending on the equation of state). Less efficient common envelopes (a large parameter α_{CE}) lead to a noticeably larger percentage of events with astrophysically interesting EM energy release. For binaries with a large mass ratio, in which a magnetized neutron star is not subjected to tidal disruption before the coalescence, the possibility of the formation of an electrically charged rotating black hole (Wald charge) is considered and estimates of the maximum EM power released by such a black hole after the coalescence are made. The conversion of the emitted gravitational waves into electromagnetic ones in the relativistic lepton plasma generated in coalescing pulsarblack hole binaries at the pre-coalescence stage is also discussed.

Keywords: gravitational waves, neutron star – black hole binaries, gamma-ray bursts

1 INTRODUCTION

The discovery of gravitational waves (GWs) from the coalescence of binary black holes (BHs) by the LIGO ground-based laser interferometers (Abbott et al. 2016b) was one of the biggest scientific discoveries at the beginning of the 21st century and gave powerful impetus to the development of multi-wavelength observations of cosmic transients. Multi-wavelength observations of the first binary neutron star (NS) coalescence GW170817 (Abbott et al. 2016a) ushered in a new era of astronomical observations – multi-messenger astronomy. At present, there is detailed information about ten coalescing binary BHs discovered by the LIGO/Virgo Collaboration during the first and second scientific run O1 and O2 (LIGO/Virgo Collaboration 2018). More than 30 coalescing binary BHs, several NS + NS binary candidates, and several NS + BH binary candidates were discovered in the ongoing O3 observations by the LVC Collaboration (see the online catalog <https://gracedb.ligo.org/latest/>). No reliable detection of the accompanying electromagnetic (EM) radiation from new coalescences in the O3 data has been reported so far. Obviously, the information about the GW coalescence source obtained from EM observations complement significantly the information obtained from an analysis of the GW signal properties. For example, the latest analysis of the GW data by the LVC Collaboration (LIGO Collaboration et al. 2019) does not rule out the possibility that one of the GW170817 binary components can be a low-mass BH, although an analysis of the EM radiation from the accompanying gamma-ray burst GRB 170817A argues for the formation of a supermassive neutron star as a result of the coalescence and, hence, for the model of two coalescing NSs in the source GW170817 (Gill et al. 2019; Piro et al. 2019).

Clearly, studying the generation mechanisms and parameters of the EM radiation during the coalescence of binary relativistic stars remains a topical problem. In this paper, we address NS + BH binary systems. Such binaries are of interest on their own because a magnetized NS before the coalescence can be a radio pulsar. An analysis of the pulse arrival time (timing) for such a pulsar in a strong BH gravitational field could provide unique information about the spacetime structure near the BH. Binary radio pulsars with BHs have been studied previously (see, e.g., Lipunov et al. 1994; Pfahl et al. 2005), but they have not yet been detected.

As relativistic numerical calculations show, the result of the NSBH coalescence in a binary system depends significantly on the component mass ratio $q = M_{BH}/M_{NS} > 1$ and the NS equation of state (Shibata and Taniguchi 2011; Shibata and Hotokezaka 2019). The neutron star can be disrupted by tidal forces before the coalescence or be swallowed by the BH entirely. A key criterion is the ratio of the tidal NS radius $R_t \sim R_{NS}q^{1/3}$ to the radius of the innermost stable circular orbit around the BH R_{ISCO} . The tidal radius depends on the mass ratio and the NS equation of state, while the radius of the innermost stable circular orbit is determined by the BH mass and angular momentum. At $R_t > R_{ISCO}$ a disk-shaped or crescent-shaped structure is formed around the BH with a possible sub-relativistic dynamic jet as a result of the coalescence

(Kyutoku et al. 2015; Shibata and Hotokezaka 2019), which is favorable for the emergence of the subsequent optical kilonova afterglow (Kawaguchi et al. 2016; Metzger 2019). After the coalescence, the BH acquires an additional angular momentum and physical conditions arise for the formation of a relativistic jet, for example, by the BlandfordZnajek (BZ) EM mechanism (Blandford and Znajek 1977), and the generation of a short gamma-ray burst (GRB) (Nakar 2007).

In our recent paper (Postnov and Kuranov 2019), we performed model calculations of the angular momenta of coalescing binary BHs for various initial spins of the components (co-aligned and randomly oriented spins), BH formation models (without any additional fallback of the stellar envelope during the collapse onto the CO core and with this fallback), and various common envelope efficiencies α_{CE} (the ratio of the binding energy of the stellar core and envelope after the main sequence to the orbital energy of the binary before the beginning of the common envelope stage) by the population synthesis method. In these calculations we used the standard scenario for the evolution of massive binary stars (Postnov and Yungelson 2014) supplemented by the treatment of the evolution of stellar core rotation with allowance made for the effective core-envelope coupling proposed in Postnov et al. (2016). The calculations were performed for various initial chemical compositions (metallicities) of stars by taking into account the time evolution of the metallicity and the star formation rate in the Universe (for details, see Postnov and Kuranov (2019)). The technique of these calculations was applied to NS+BH binaries, which allowed the coalescence rate \mathcal{R} (in $\text{yr}^{-1} \text{Gpc}^{-3}$) and the detection rate \mathcal{D} (in yr^{-1}) at the sensitivity level of the operating GW interferometers to be calculated (Postnov et al. 2019).

In the present paper, the mass ratios $q = M_{BH}/M_{NS}$ and the BH spins before the coalescence of NS+BH binaries obtained in our calculations (Postnov et al. 2019) are used as input parameters to determine the mass of the remnant disk around the BH M_d and the BH spin (characterized by the dimensionless Kerr parameter $a^* = J_{BH}/(GM_{BH}^2/c^2)$, J_{BH} is the BH angular momentum, G is the gravitational constant, and c is the speed of light) after the coalescence. The disk mass depends significantly on the NS compactness (mass-to-radius ratio M_{NS}/R_{NS}), which is defined by the NS equation of state. The effects of the equation of state are parameterized by the tidal deformability $\Lambda = (2/3)k_2[(c^2/G)(R_{NS}/M_{NS})]^5$ (Damour et al. 2012) (k_2 is the Love number). This parameter is constrained from the GW observations of the source GW170817 (Abbott et al. 2019).

In turn, the disk mass and the BH spin determine the possible kinetic energy of the relativistic jet launched by the BZ mechanism. The kinetic energy of the jet ΔE_{BZ} may be considered as an upper limit for the isotropic energy of a short GRB ΔE_{iso} . For coalescing binaries with a large mass ratio q , in which the NS is swallowed by the BH without disruption, the NS magnetic field and the BH spin after the coalescence a^* are used to calculate the possible BH electric charge in the NS magnetic field (Wald 1974). In addition, if the NS before the coalescence was at the radio pulsar stage, then the medium around the coalescing NS+BH binary could be filled with a relativistic lepton plasma. We also consider the

mechanism for the conversion of gravitational waves into electromagnetic ones in such a magnetized relativistic plasma.

2 COALESCENCE AND DETECTION RATES OF NS+BH BINARIES WITH GW INTERFEROMETERS

Figure 1 shows the results of our population synthesis calculations of the NS+BH binary coalescence rate density and the detection rates by the LIGO/Virgo ground-based laser GW interferometers. The parameters of the NS and BH formation, the evolution of massive binary systems, and the technique of calculations are described in detail in Postnov and Kuranov (2019) and Postnov et al. (2019). At the coalescence phase, the GW signal amplitude is determined by the chirp mass of the binary system, which for two point masses M_1 and M_2 is $\mathcal{M} = (M_1 M_2)^{3/5} / (M_1 + M_2)^{1/5}$. The detection horizon D_h of coalescing binary systems with a chirp mass $\mathcal{M} = 1.22 M_\odot$ for two neutron stars with a canonical mass of $1.4 M_\odot$ in the current LIGO/Virgo observations is taken to be 120 Mpc. The detection horizon depends on the binary chirp mass as $D_h \sim \mathcal{M}^{5/6}$ (LIGO Collaboration et al. 2010).

The distribution of parameters for binaries that can be recorded by the ground-based GW interferometers within the detection horizon D_h is important from the viewpoint of comparison with observations. At a given sensitivity level of the GW detectors, D_h is determined mainly by the chirp mass. Thus, for each chirp mass there is a limiting distance (redshift) to which the binary coalescence rate density \mathcal{R}_{NSBH} calculated by the population synthesis method should be integrated. In turn, the coalescence rate per unit comoving volume $\mathcal{R}_{NSBH}(t)$ is a convolution of the calculated time dependence of the binary system coalescence rate $\mathcal{R}_\delta(t)$ calculated for an instantaneous star formation burst with the star formation rate and the stellar metallicity as functions of time $SFR(t)$: $\mathcal{R}_X(t) = \int^t SFR(t - \tau) \mathcal{R}_\delta(\tau) d\tau$. The time evolution of the metallicity of the stellar population and the star formation rate were calculated using the formulas given in Postnov and Kuranov (2019).

It can be seen from Fig. 1 that the expected detection rate of NS+BH binaries is approximately several events per year, which is consistent with the existing detection statistics of such binaries (for the online information about the detected events, see <https://gracedb.ligo.org/latest/>).

3 COALESCENCES WITH NS TIDAL DISRUPTION

The NS+BH binary coalescences in which the NS is tidally disrupted are most interesting from the standpoint of observational manifestations in the EM range. As was said in the Introduction, the NS tidal disruption occurs mostly in binaries with a small component mass ratio $q = M_{BH}/M_{NS} \lesssim 3$ and depends on the NS equation of state (tidal deformability Λ).

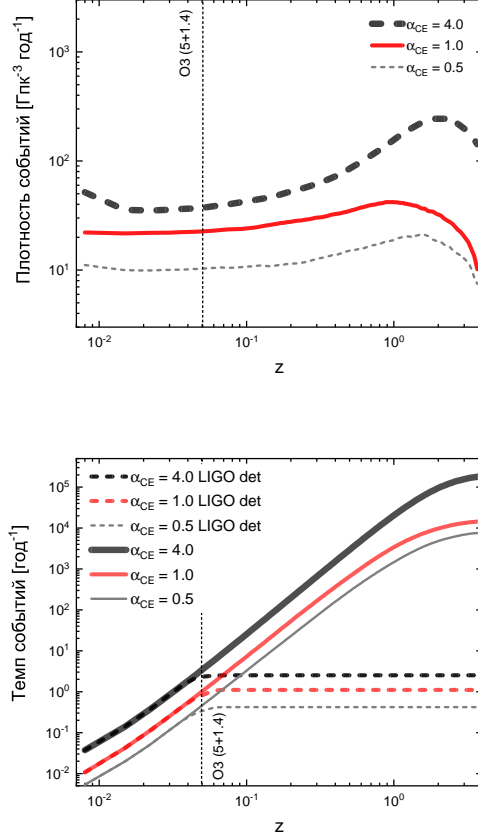


Fig. 1: Upper panel: NS+BH coalescence rate density \mathcal{R}_{NSBH} (per year per cubic Gpc) versus cosmological redshift z for various values of the parameter α_{CE} (common envelope efficiency) with allowance made for the evolution of the mean star formation rate and the stellar metallicity in the Universe. The upper and lower boundaries (dashed lines) correspond to $\alpha_{CE} = 4$ and 0.5 , respectively; the solid line corresponds to $\alpha_{CE} = 4$. The vertical dashed line indicates the LIGO/Virgo O3 detection horizon for coalescing binary systems with masses of $5+1.4 M_{\odot}$. Bottom panel: Number of NS+BH coalescences per year (the integral of the coalescence rate per unit volume to the distance corresponding to a given z) versus limiting redshift (detection horizon D_h) with allowance made for the star formation history in the Universe for common envelope efficiencies $\alpha_{CE} = 0.5, 1, 4$. The dashed curve indicates the expected number of events per year detected by the LIGO/Virgo O3 interferometers for the averaged orientation of the binary orbits relative to the line of sight $\mathcal{R}_{BHNS} \sim 1 - 3 \text{ yr}^{-1}$. The vertical dashed line indicates the LIGO/Virgo O3 detection horizon for coalescing binary systems with masses of $5+1.4 M_{\odot}$.

3.1 Remnant Disks around the BH

To estimate the mass of the baryonic disk (torus) around the BH left after the coalescence, we will use the fit to the numerical data with allowance made for the NS equation of state that has been proposed recently (Zappa et al. 2019). In turn, the fitting formulas in this paper use the results from Jimenez-Forteza et al. (2017), where the radiated GW energy, the mass and spin of the BH remaining after the coalescence of binary BHs with a different mass ratio are calculated.

The derived mass ratio distributions of NS+BH binaries are presented in Fig. 2. The upper three rows in this and next figures present the simulation results for stellar metallicities in the ranges $Z > 0.01$, $0.01Z > 0.001$ and $0.001Z > 0.0001$ (from top to bottom), while the lower row presents the convolution with the time evolution of the metallicity.

The left and right columns in the figure present the calculations, respectively, for the standard common envelope efficiency $\alpha_{CE} = 1$ and $\alpha_{CE} = 4$ corresponding to a smaller approach of the binary components in the common envelope. Note that the reduced common envelope efficiency $\alpha_{CE} = 4$ corresponds better to the treatment of the binary dynamics in the common envelope based on the angular momentum conservation law (the so-called γ -formalism; see Nelemans and Tout 2005) and is required to explain the properties of the population of symbiotic X-ray binary systems in the Galaxy (Yungelson et al. 2019). It can be seen from Fig. 2 that in $\sim 10 - 20\%$ of the coalescences the component mass ratio is small enough for the formation of a remnant disk around the BH after the coalescence.

The BH spin after the coalescence of NS+BH binaries is entirely determined by the initial BH spin a^* and the mass ratio q and depends weakly on the NS equation of state. The distribution in initial BH spins (before the coalescence) calculated by Postnov et al. (2019) is indicated in Fig. 3 by the dotted line, while the spins after the coalescence a_f^* are indicated by the solid line. The BH spins after the coalescence are seen to be concentrated near $a_f^* \sim 0.5$, while the fraction of rapidly rotating BHs after the coalescence is small.

The resulting mass of the disk around the BH after NS tidal disruption is shown in Fig. 4 for various values of the NS tidal deformability Λ in the wide range from 100 to 2000 spanning a broad spectrum of possible NS equation of state (LIGO Collaboration et al. 2019). We see a strong dependence of the disk mass on the NS equation of state – astrophysically interesting disk masses $M_d > 0.05M_\odot$ are obtained only at large $\Lambda > 300$ corresponding to small compactness M_{NS}/R_{NS} (stiff equations of state). Note that the constraints on the parameter Λ from the GW observations of GW170817 lie within a wide range, but significant tidal deformations with $\Lambda \gtrsim 1600$ are highly unlikely (Abbott et al. 2019; LIGO Collaboration et al. 2019). An independent analysis with the involvement of other constraints gives $\Lambda = 390_{-210}^{+280}$ for the mass $M_{NS} = 1.4M_\odot$ (Jiang et al. 2019).

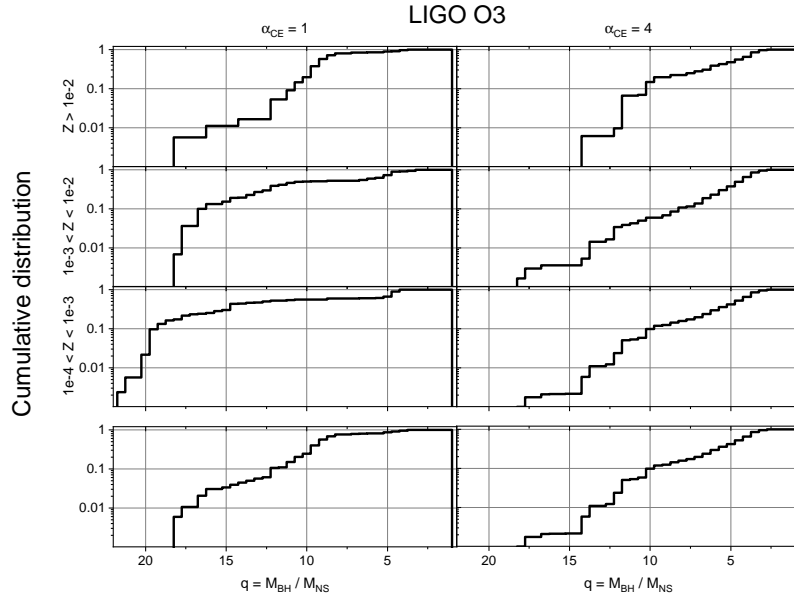


Fig. 2: Cumulative distribution in mass ratio in coalescing NS+BH binaries that can be recorded at the sensitivity level of the LIGO/Virgo GW detectors in the observing run O3. The upper three rows present the results for various stellar metallicities. The fourth row presents the result with allowance made for the time evolution of the mean star formation rate and the stellar metallicity in galaxies. The left and right columns present the calculations for the common envelope parameters $\alpha_{CE} = 1$ and 4, respectively.

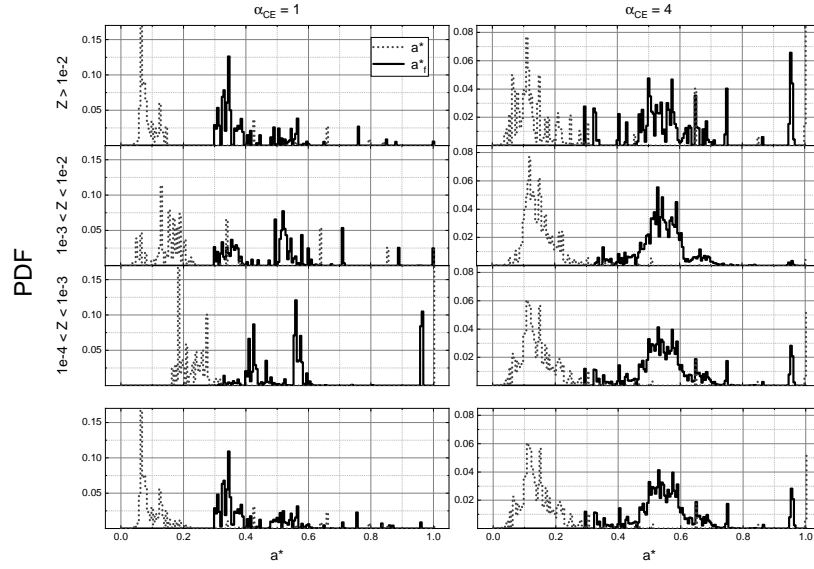


Fig. 3: BH spins before (a^* , dotted line) and after the coalescence (a_f^* , solid line) in NS+BH binaries. The dependence on the NS equation of state is indistinguishable. The upper three rows present the results for various stellar metallicities Z . The fourth row presents the convolution with allowance made for the time evolution of the mean star formation rate and the stellar metallicity in galaxies. The left and right columns present the calculations for the common envelope parameters $\alpha_{CE} = 1$ and 4, respectively.

3.2 Jet kinetic energy

The minimum isotropic kinetic energy of the relativistic jet required to produce a GRB is estimated from observations as $\Delta E_{K,min} \simeq 10^{48}$ erg (Soderberg et al. 2006). An analysis of the observations of short GRBs shows that the mean conversion efficiency of the kinetic energy of the relativistic jet into gamma-ray emission is $\eta = E_{\gamma,iso}/(E_{\gamma,iso} + E_{K,iso}) \sim 0.4$ (with a large scatter of individual sources) (Fong et al. 2015). This allows the kinetic energy of the jet to be used to estimate the possible power of the short GRB produced by it.

To be specific, consider the BlandfordZnajek process as a possible physical mechanism of a short GRB (Nakar 2007). The energy of the BZ jet is determined by the magnetic field around the BH and its spin, $L_{BZ} \sim \Phi^2 \Omega_H^{*2} f(\Omega_H^*)$, where Φ is the magnetic flux through the BH ergosphere, $\Omega_H^* = (1/2)a^*/(1 + \sqrt{1 - a^{*2}})$ is the dimensionless angular velocity of rotation on the BH horizon, and $f(\Omega_H^*) \approx 1 + 1.38\Omega_H^{*2} - 9.2\Omega_H^{*4}$ is the correction function that can be derived by fitting the numerical calculations (Nakar 2007). The magnetic field is an uncertain parameter, but it can be eliminated by assuming the balance between the magnetic and dynamic pressures in the disk around the BH. In this case, $L_{BZ} \sim \dot{M}c^2\Omega_H^{*2}f(\Omega_H^*)$. Assuming the accretion rate to be $\dot{M} = M_d/\Delta t$, where Δt is the accretion time, the kinetic energy of the BZ jet is found to be $\Delta E_{K,iso} \approx 0.015M_dc^2\Omega_H^2f(\Omega_H)$ (we use the numerical coefficient justified in Barbieri et al. 2019).

Figure 5 presents the cumulative distributions of the kinetic energy of the BZ jet $\Delta E_{K,iso}$ for coalescing NS+BH binary systems within the detection horizon $D_h(O3)$ at the current phase of O3 observations with the LIGO/Virgo GW interferometers with allowance made for the evolution of the metallicity Z and the mean star formation rate SFR in galaxies for two common envelope parameters. We see a strong dependence on the NS equation of state (more energetic jets are obtained at greater values of the tidal deformability Λ) and on the degree of approach of the binary components at the common envelope stage. Less efficient common envelopes (a large parameter α_{CE}) lead to a noticeably larger percentage events with astrophysically interesting EM energy release

4 COALESCENCES WITHOUT NS TIDAL DISRUPTION

The NS+BH coalescences in binaries with a large mass ratio q occurring without tidal disruption can also be of interest from the viewpoint of the appearance of accompanying EM radiation. The NS should have a magnetic field, with the NS+BH coalescences occurring in a fairly short time after the formation in most cases, so that the NS magnetic field has no time to decay. Several physical mechanisms for the generation of EM radiation associated with electrodynamic processes in the vicinity of a BH coalescing with a magnetized NS (see, e.g., Zhang 2016; Levin et al. 2018; Zhang 2019; Dai 2019; and references therein) or with the fundamental graviton-to-photon conversion in a magnetic field (Dolgov and Postnov 2017) are possible in this case.

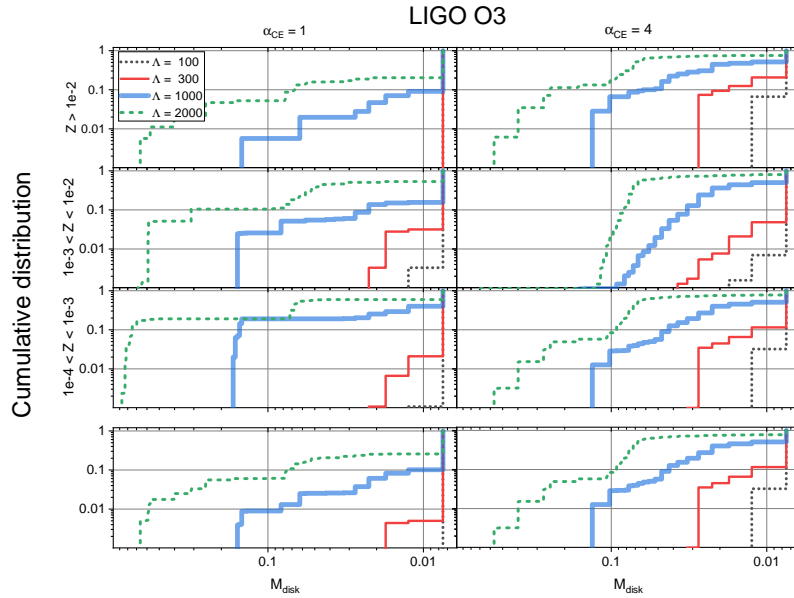


Fig. 4: (Color online) Cumulative distributions of the mass of the remnant disk around the BH after NS tidal disruption. The color lines in the inset indicate the NS tidal deformability Λ parameterizing the various NS equations of state. The upper three rows present the results for various stellar metallicities. The fourth row presents the result with allowance made for the time evolution of the mean star formation rate and the stellar metallicity in galaxies. The left and right columns present the calculations for the common envelope parameters $\alpha_{CE} = 1$ and $\alpha_{CE} = 4$, respectively.

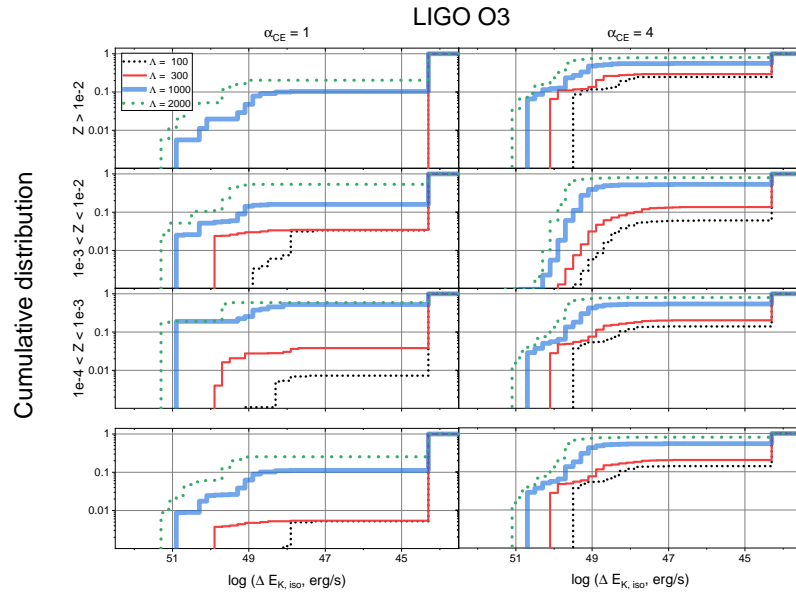


Fig. 5: (Color online) Same as Fig. 4, but for the kinetic energy of the jet launched by the BlandfordZnajek mechanism from the remnant disk around the rotating BH after the coalescence of NS+BH binaries.

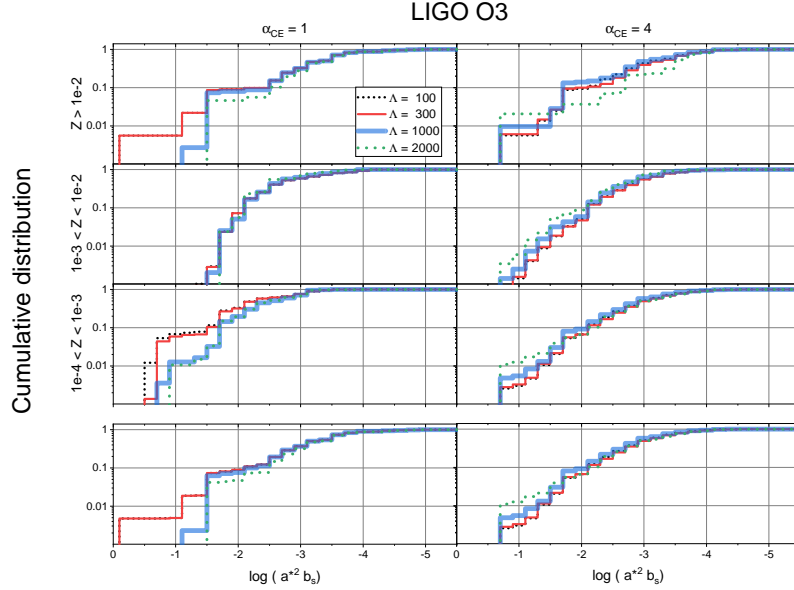


Fig. 6: (Color online) Same as Fig. 4, but for the combination of the BH spin before the coalescence and the NS magnetic field a^*b_s determining the maximum intrinsic magnetic dipole moment of a Wald-charged BH $\mu_{W,max}$ (Eq. (2)).

4.1 Electric Charge of a Rotating BH

The spin and orbital motion of an electrically charged BH in a coalescing binary system initiate time-varying electric dipole and magnetic dipole moments in the binary that give rise to EM radiation (for the estimates and discussion, see Dai 2019), whose power and energetics for rapidly rotating BHs can be sufficient for the explanation of short EM transients (for example, fast radio bursts (FRBs); see Popov et al. 2018)). A rotating BH in an external magnetic field can acquire an electric charge with a maximum value of $Q_w = (2G/c^3)JB$, where $J = a^*GM_{BH}^2/c$ is the angular momentum of the rotating BH and B is the magnetic field strength (Wald 1974). This mechanism has also been recently discussed for the estimates of a possible EM radiation pulse already after the NS+BH coalescence (Zhong et al. 2019). It is convenient to normalize the charge of a rotating ReissnerNordström BH to the characteristic value of $Q_{RN} = 2\sqrt{GM_{BH}} \approx 10^{30}(M_{BH}/M_{\odot})$ (emu) corresponding to the equality of the Schwarzschild radius to the ReissnerNordström radius: $\tilde{q}_w = Q_w/Q_{RN}$.

In natural units $\hbar = c = 1$ Newtons gravitational constant is written via the Planck mass $G = 1/m_{Pl}^2$, $m_{Pl} \approx 10^{19}$ GeV, the electric charge is dimensionless, the electron charge is expressed via the fine structure constant $\alpha = 1/137$ as

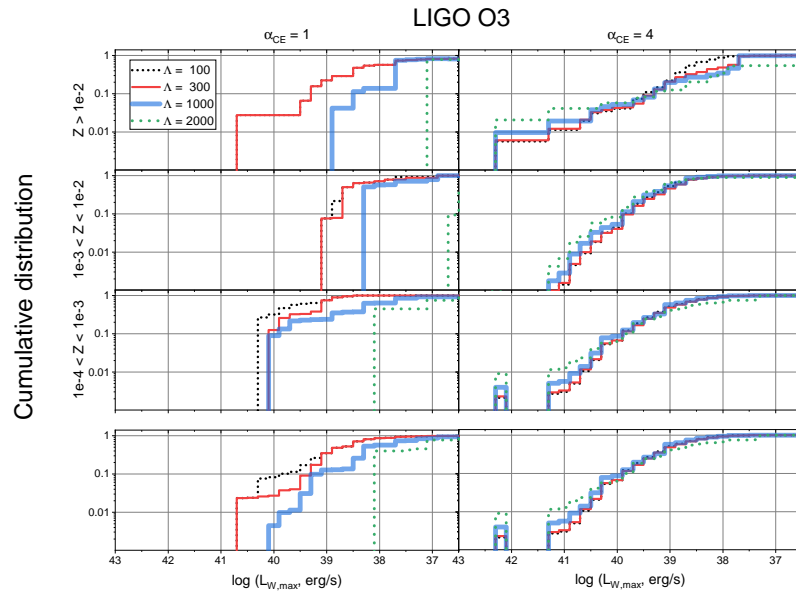


Fig. 7: (Color online) Same as Fig. 4, but for the maximum energy release from a charged rotating BH after the coalescence $L_{W,max}$ (Eq. (3)).

$e^2 = 4\pi\alpha$. It is also convenient to make the magnetic field dimensionless by normalizing it to the critical (Schwinger) one $b = B/B_{cr}$, where $B_{cr} = m_e^2/e \approx 4.41 \times 10^{13}$ G ($m_e \approx 511$ keV is the electron rest mass). The specific Wald BH charge is then

$$\tilde{q}_W = \frac{a^*b}{\sqrt{4\pi\alpha}} \left(\frac{m_e}{m_{Pl}} \right)^2 \left(\frac{M_{BH}}{m_{Pl}} \right) \approx 10^{-6} a^*b \left(\frac{M_{BH}}{M_\odot} \right). \quad (1)$$

This formula is written for a uniform magnetic field. Note that for a NS dipole field $b(R) = b_s(R_{NS}/R)^3$, where b_s is the surface field, it follows from (1) that at the tidal radius $R_t \sim R_{NS}q^{1/3}$ the specific Wald charge does not depend on the BH mass: $\tilde{q}_W \sim 10^{-6} a^*b_s(M_{NS}/M_\odot)$.

For the electric dipole and magnetic dipole radiation associated with the orbital motion of a charged BH before the coalescence, the EM radiation power is proportional to the square of the NS magnetic field b and the square of the BH spin, $\sim a^{*2}b^2$. In the case of magnetic dipole radiation from the rotating charged BH itself acquiring the Wald charge at the stage when the charged NS approaches the BH before the coalescence, it is proportional to the square of the intrinsic magnetic moment $\mu_W^2 \sim a^{*4}b^2$ (Dai 2019). Therefore, the Wald charge can be important only for rapidly rotating BHs with $a^* \gtrsim 0.5$. The number of such binaries before the coalescence is extremely small (see the dashed curve in Fig. 3).

If the NS is swallowed by the BH without being disrupted, the maximum Wald charge can be estimated from the magnetic field at the Schwarzschild BH radius $R \sim R_g = 2GM_{BH}/c^2$ before the coalescence: $\tilde{q}_{W,max} \sim 3 \times 10^{-5} a^*b_s(R_{NS}/10\text{km})^3(M_{BH}/M_\odot)^{-2}$. In this case, the maximum intrinsic magnetic dipole moment of the charged BH will be determined only by the BH spin a^* , NS magnetic field b_s , and NS radius:

$$\mu_{W,max} = \frac{J_{BH}Q_{W,max}}{M_{BH}c} \approx 5 \times 10^{30} a^{*2}b_s \left(\frac{R_{NS}}{10\text{km}} \right)^3. \quad (2)$$

The maximum energy release from a charged rotating single BH with a magnetic moment $\mu_{W,max}$ can be estimated from the magnetic dipole formula $L_{W,max} \sim \mu_{W,max}^2 \Omega_H^4$, where $\Omega_H^f \sim (a_f^*/2)(c^3/GM_{BH}^f)$ is the angular velocity of the horizon for a BH with mass M_{BH}^f BH after the coalescence. Substituting $\mu_{W,max}$ from (2), we find

$$L_{W,max} \sim 10^{42} [\text{erg/s}] a^{*4} b_s^2 a_f^{*4} \frac{(R_{NS}/10\text{km})^6}{(M_{BH}^f/10M_\odot)^4}. \quad (3)$$

This estimate is comparable in magnitude to the estimates of the possible EM energy release from charged BHs at the pre-coalescence (in-spiraling) stage (Zhang 2019; Dai 2019). Given the relative smallness of the BH spins before ($a^* \sim 0.2$, the dashed curve in Fig. 3) and after ($a^{*f} \sim 0.6$ the solid curve in Fig. 3) the coalescence as well as the low (poorly known) Poynting flux-to-EM radiation conversion efficiency, there can be astrophysically interesting EM

energy release in this process only for rapidly rotating low-mass BHs in a pair with strongly magnetized NSs with $b_s \sim 1$, whose number is extremely small.

4.2 Conversion of Gravitational Waves in a Relativistic Plasma in a Magnetic Field

At the final stages before the coalescence of a binary magnetized NS+BH, conditions for the additional appearance of EM radiation due to the coherent conversion of gravitational waves into electromagnetic ones in a magnetic field arise in the binary. For a vacuum this mechanism was first considered by Gertsenshtein (1962). In the presence of a surrounding plasma the effect in cosmological applications was considered by Dolgov and Ejlli (2012), while for the case of conversion in a nonrelativistic plasma with a magnetic field around astrophysical GW sources, coalescing binary NSs and BHs, it was considered by Dolgov and Postnov (2017). In the latter paper it was emphasized that since the plasma frequency in the interstellar medium with density $n_e \sim 1 \text{ cm}^{-3}$, $\Omega_e = 60 \sqrt{n_e}$ kHz, is much greater than the frequency of the GWs from coalescing binary systems (100 200 Hz), then the GW-to-EM conversion in the plasma is dissipative in nature and is determined by the imaginary part of the dielectric permittivity. The EM wave damping amplitude A_j was shown to be related to the amplitude h_j of a GW propagating with frequency ω perpendicularly to an external magnetic field B by the relation (in natural units $\hbar = c = k_B = 1$)

$$A_j \approx \frac{\kappa b \omega a_e}{\Omega_e} h_j, \quad (4)$$

where $a_e = \sqrt{\frac{T_e}{e^2 n_e}}$ is the Debye radius of electrons, T_e is the electron temperature, $\kappa^2 = 16\pi/m_{Pl}^2$ is the coupling constant.

The fraction of the energy being released in the GW that dissipates into the thermal energy of the plasma,

$$K_{nr} = \left(\frac{\kappa B \omega a_e}{\Omega_e} \right)^2 \approx 10^{-46} \left(\frac{\omega}{\Omega_e} \right)^2 \left(\frac{a_e}{\text{cm}} \right)^2 \left(\frac{B}{1 \text{ G}} \right)^2 \quad (5)$$

is very small and is interesting only for superstrong magnetic fields. It may well be that part of this energy can be reprocessed into high-frequency radio emission (Marklund et al. 2000).

During the coalescence of magnetized NSs with BHs, the magnetosphere of a NS with a magnetic field B_{NS} spinning with a frequency $\omega_{NS} = 2\pi/P_{NS}$ is filled with an ultrarelativistic plasma with a density no less than the Goldreich-Julian charge density $n_{GJ} = (\omega_{NS} B_{NS})/(2\pi e)$. For radio pulsars $n_e = \lambda n_{GJ}$, where $\lambda \sim 10^4 - 10^5$ is the multiplicity factor of the pairs created near the NS surface (Beskin 2018). In a relativistic collisional plasma with a plasma frequency $\Omega_{rel}^2 = \frac{4\pi e^2 n_e}{3T_e}$, $T_e \sim \gamma m_e$ (γ is the electron Lorentz factor) we can obtain (Postnov and Simkin 2019)

$$A_j \approx \frac{\kappa b \omega}{\Omega_{rel}^2} h_j \sim \frac{\kappa b \omega}{(n_e/\gamma m_e)}. \quad (6)$$

If the plasma flows along open magnetic field lines (as in a pulsar), then for a dipole field $B(R) \sim B_s(R_{NS}/R)^3$. In a magnetic flux tube the magnetic flux is conserved, $\Phi = B(R)S(R) = \text{const}$; given the continuity equation $n_e B(R)S(R) = \text{const}$, we then find that for an ultrarelativistic collisional plasma with $T_e \sim \gamma m_e$ the conversion efficiency does not depend on the NS magnetic field, but is determined only by the lepton Lorentz factor, the NS spin period, and the pair multiplicity with respect to the Goldreich-Julian density λ :

$$K_{rel} = \left(\frac{\kappa b \omega}{\Omega_{rel}^2} \right)^2 \approx 10^{-35} \left(\frac{\omega}{100 \text{ rad s}^{-1}} \right)^2 \left(\frac{P_{NS}}{1 \text{ s}} \right)^2 \left(\frac{\lambda}{10^5} \right)^{-2} \left(\frac{\gamma}{10^5} \right)^2. \quad (7)$$

Clearly, the effect is weak for the densities of a relativistic pulsar plasma with $\lambda \sim 10^4 - 10^5$. However, the relativistic plasma density near a coalescing NS+BH binary is unknown and, therefore, the density n_{GJ} can serve only as an approximate lower limit. The upper bound of the GW-to-EM conversion efficiency in a relativistic plasma around a coalescing NS+BH binary will then be $K_{rel} \lesssim 10^{-25} (P_{NS}/1\text{s})^2 (\gamma/10^5)^2 (n_e/n_{GJ})^{-2}$, i.e., for a GW pulse energy during the coalescence of $M_\odot c^2 \sim 2 \times 10^{54}$ erg, up to $\sim 10^{38}$ ergs can be additionally reprocessed into the thermal energy of the plasma.

5 CONCLUSION

In this paper we analyzed the various physical mechanisms that could give rise to an EM pulse accompanying the coalescence of magnetized NS+BH binaries. At the time of writing this paper (mid- October 2019), the LIGO/Virgo detectors recorded several such binaries, but no EM radiation from them have been detected so far. Based on a series of population synthesis calculations (Postnov and Kuranov 2019; Postnov et al. 2019), we constructed the distributions of the NS+BH binary coalescence rate density and the expected detection rate of such binaries in the current LIGO/Virgo O3 observations by taking into account the evolution of the stellar metallicity and the star formation rate in the Universe (Fig. 1).

The derived distributions of coalescing NS + BH in component mass ratio $q = M_{BH}/M_{NS} > 1$, magnetic fields $b_s = B_{NS}/B_{cr}$, $B_{cr} = 4.14 \times 10^{13}$ G, NS spin period, and BH angular momentum (dimensionless spin $a^* = J_{BH}/(GM_{BH}^2/c)$) before the coalescence were used to estimate the mass of the remnant disk around the BHmd (Fig. 4) and the BH spin after the coalescence a_f^* (Fig. 3). We estimated the masses of the remnant baryonic disks, the BH masses and spins after the coalescence based on interpolation of the relativistic numerical calculations by Zappa et al. (2019) and Jimenez-Forteza et al. (2017) by taking into account the NS equation of state that was specified by the dimensionless tidal deformability Λ . Assuming that the magnetic field in the remnant disk around a rotating BH to be dynamically balanced, we estimated the kinetic energy of the relativistic jet launched by the BZ mechanism (Fig. 5), which depends strongly on the NS equation of state through the tidal deformability Λ .

We separately studied the NS+BH coalescences with a large mass ratio q occurring without NS tidal disruption. For such binaries we constructed the distributions of the maximum possible BH magnetic dipole moment before the coalescence $\mu_{W,max}$ acquired due to the Wald BH charge (Wald 1974; Levin et al. 2018) (Fig. 6) and corresponding to the maximum EM magnetic dipole luminosity of such a charged BH $L_{W,max}$ (Fig. 7). Even for the most optimistic parameters our estimates of the EM luminosity from a Wald-charged BH in coalescing NS+BH binaries are considerably smaller than those expected from binaries with a smaller mass ratio, where the formation of remnant disks and relativistic jets is possible.

We additionally considered the conversion of gravitational waves in a magnetic field with a relativistic plasma that may surround a NS+BH binary at the pre-coalescence stage. This mechanism was shown to convert no more than $\sim 10^{38} - 10^{39}$ erg into additional plasma heating even under the most favorable conditions (a large lepton Lorentz factor $\gamma \sim 10^5$ and a low plasma density of the order of the Goldreich-Julian one).

Our general conclusion is that noticeable EM phenomena from coalescing NS+BH binaries might be expected from a small fraction of the coalescences in which the NS is tidally disrupted and a remnant disk is formed around the rotating BH. The fraction of such events depends on the mass ratio q and the NS equation of state. At the expected coalescence rate of several events per year in the current LIGO/Virgo O3 GW observations, the chances to see a weak EM signal are slim. The more exotic physical mechanisms (the Wald electric charge of a rotating BH or the fundamental conversion of gravitational waves into electromagnetic ones in a magnetized plasma surrounding a coalescing NS+BH binary) are much less efficient. At the current detector sensitivity level EM phenomena from coalescing NS+BH binaries in various ranges might be expected only from the nearest events (at distances of tens of Mpc). The detection of an EM counterpart from NS+BH can potentially give physically rich information about the equation of state and the magnetic field of neutron stars.

Acknowledgements. The work of K.A. Postnov was supported by RSF grant no. 19-12-00229. The work of A.G. Kuranov was supported by the Scientific School of the Moscow State University Physics of Stars, Relativistic Objects, and Galaxies.

References

1. B. P. Abbott, R. Abbott, T. D. Abbott, et al., Phys. Rev. Lett. 116, 241103 (2016a).
2. B. P. Abbott, R. Abbott, T. D. Abbott, et al., Phys. Rev. Lett. 116, 061102 (2016b).
3. B. P. Abbott, R. Abbott, T. D. Abbott, LIGO Sci. Collab., and Virgo Collab., Phys. Rev. X 9, 011001 (2019).
4. C. Barbieri, O. S. Salafia, A. Perego, M. Colpi, and G. Ghirlanda,

arXiv:1908.08822 (2019).

5. V. S. Beskin, *Phys. Usp.* 61, 353 (2018).
6. R. D. Blandford and R. L. Znajek, *Mon. Not. R. Astron. Soc.* 179, 433 (1977).
7. Z. G. Dai, *Astrophys. J. Lett.* 873, L13 (2019).
8. T. Damour, A. Nagar, and L. Villain, *Phys. Rev. D* 85, 123007 (2012).
9. A. D. Dolgov and D. Ejlli, *J. Cosmol. Astropart. Phys.* 2012 (12), 003 (2012).
10. A. Dolgov and K. Postnov, *J. Cosmol. Astropart. Phys.* 2017 (9), 018 (2017).
11. W. Fong, E. Berger, R. Margutti, and B. A. Zauderer, *Astrophys. J.* 815, 102 (2015).
12. M. Gertsenshtein, *Sov. Phys. JETP* 14, 84 (1962).
13. R. Gill, A. Nathanail, and L. Rezzolla, *Astrophys. J.* 876, 139 (2019).
14. J.-L. Jiang, S.-P. Tang, D.-S. Shao, et al., arXiv:1909.06944 (2019).
15. X. Jimenez-Forteza, D. Keitel, S. Husa, et al., *Phys. Rev. D* 95, 064024 (2017).
16. K. Kawaguchi, K. Kyutoku, M. Shibata, and M. Tanaka, *Astrophys. J.* 825, 52 (2016).
17. K. Kyutoku, K. Ioka, H. Okawa, M. Shibata, and K. Taniguchi, *Phys. Rev. D* 92, 044028 (2015).
18. J. Levin, D. J. D’Orazio, and S. Garcia-Saenz, *Phys. Rev. D* 98, 123002 (2018).
19. LIGO/Virgo Sci. Collab., arXiv e-prints (2018).
20. The LIGO Sci. Collab., the Virgo Collab., J. Abadie, et al., arXiv:1003.2481 (2010).
21. The LIGO Sci. Collab., the Virgo Collab., et al., arXiv:1908.01012 (2019).
22. V. M. Lipunov, K. A. Postnov, M. E. Prokhorov, and E. Y. Osminkin, *Astrophys. J.* 423, L121 (1994).
23. M. Marklund, G. Brodin, and P. K. S. Dunsby, *Astrophys. J.* 536, 875 (2000).
24. B. D. Metzger, arXiv:1910.01617 (2019).
25. E. Nakar, *Phys. Rep.* 442, 166 (2007).
26. G. Nelemans and C. A. Tout, *Mon. Not. R. Astron. Soc.* 356, 753 (2005).
27. E. Pfahl, P. Podsiadlowski, and S. Rappaport, *Astrophys. J.* 628, 343 (2005).
28. L. Piro, E. Troja, B. Zhang, et al., *Mon. Not. R. Astron. Soc.* 483, 1912 (2019).
29. S. B. Popov, K. A. Postnov, and M. S. Pshirkov, *Phys. Usp.* 61, 965 (2018).
30. K. Postnov, A. Kuranov, and N. Mitichkin, *Phys. Usp.* 62, 1153, (2019); arXiv:1907.04218 (2019).
31. K. A. Postnov and A. G. Kuranov, *Mon. Not. R. Astron. Soc.* 483, 3288 (2019).

32. K. A. Postnov and I. V. Simkin, *Journal of Physics: Conf. Ser.* 1390, 012086 (2019).
33. K. A. Postnov and L. R. Yungelson, *Liv. Rev. Relativ.* 17, 3 (2014).
34. K. A. Postnov, A. G. Kuranov, D. A. Kolesnikov, S. B. Popov, and N. K. Porayko, *Mon. Not. R. Astron. Soc.* 463, 1642 (2016).
35. M. Shibata and K. Hotokezaka, *Ann. Rev. Nucl. Part. Sci.* 69, (2019).
36. M. Shibata and K. Taniguchi, *Liv. Rev. Relativ.* 14,6 (2011).
37. A. M. Soderberg, S. R. Kulkarni, E. Nakar, et al., *Nature (London, U.K.)* 442 (7106), 1014 (2006).
38. A. Tchekhovskoy, R. Narayan, and J. C. McKinney, *Astrophys. J.* 711, 50 (2010).
39. R. M. Wald, *Phys. Rev. D* 10, 1680 (1974).
40. L. R. Yungelson, A. G. Kuranov, and K. A. Postnov, *Mon. Not. R. Astron. Soc.* 485, 851 (2019).
41. F. Zappa, S. Bernuzzi, F. Pannarale, M. Mapelli, and N. Giacobbo, *Phys. Rev. Lett.* 123, 041102 (2019).
42. B. Zhang, *Astrophys. J. Lett.* 827, L31 (2016).
43. B. Zhang, *Astrophys. J. Lett.* 873, L9 (2019).
44. S.-Q. Zhong, Z.-G. Dai, and C.-M. Deng, *arXiv:1909.00494* (2019).